Am J Physiol Lung Cell Mol Physiol 289: L338–L348, 2005.
First published April 29, 2005; doi:10.1152/ajplung.00328.2004.

Multiple ryanodine receptor subtypes and heterogeneous ryanodine receptor-gated Ca^{2+} stores in pulmonary arterial smooth muscle cells

Xiao-Ru Yang,[1] Mo-Jun Lin,[1] Kay-Pong Yip,[2] Loice H. Jeyakumar,[3] Sidney Fleischer,[3] George P. H. Leung,[1] and James S. K. Sham[1]

[1]*Division of Pulmonary and Critical Care Medicine, Johns Hopkins School of Medicine, Baltimore, Maryland;*
[2]*Department of Physiology and Biophysics, University of South Florida, Tampa, Florida;*
and [3]*Department of Biological Sciences, Vanderbilt University, Nashville, Tennessee*

Submitted 1 September 2004; accepted in final form 17 April 2005

Yang, Xiao-Ru, Mo-Jun Lin, Kay-Pong Yip, Loice H. Jeyakumar, Sidney Fleischer, George P. H. Leung, and James S. K. Sham. Multiple ryanodine receptor subtypes and heterogeneous ryanodine receptor-gated Ca^{2+} stores in pulmonary arterial smooth muscle cells. *Am J Physiol Lung Cell Mol Physiol* 289: L338–L348, 2005. First published April 29, 2005; doi:10.1152/ajplung.00328.2004.—Ryanodine receptors (RyRs) of pulmonary arterial smooth muscle cells (PASMCs) play important roles in major physiological processes such as hypoxic pulmonary vasoconstriction and perinatal pulmonary vasodilatation. Recent studies show that three subtypes of RyRs are coexpressed and RyR-gated Ca^{2+} stores are distributed heterogeneously in systemic vascular myocytes. However, the molecular identity and subcellular distribution of RyRs have not been examined in PASMCs. In this study we detected mRNA and proteins of all three subtypes in rat intralobar PASMCs using RT-PCR and Western blot. Quantitative real-time RT-PCR showed that RyR2 mRNA was most abundant, ~15–20 times more than the other two subtypes. Confocal fluorescence microscopy revealed that RyRs labeled with BODIPY TR-X ryanodine were localized in the peripheral and perinuclear regions and were colocalized with sarcoplasmic reticulum labeled with Fluo-5N. Immunostaining showed that the subsarcolemmal regions exhibited clear signals of RyR1 and RyR2, whereas the perinuclear compartments contained mainly RyR1 and RyR3. Ca^{2+} sparks were recorded in both regions, and their activities were enhanced by a subthreshold concentration of caffeine or by endothelin-1, indicating functional RyR-gated Ca^{2+} stores. Moreover, 18% of the perinuclear sparks were prolonged [full duration/half-maximum (FDHM) = 193.3 ± 22.6 ms] with noninactivating kinetics, in sharp contrast to the typical fast inactivating Ca^{2+} sparks (FDHM = 44.6 ± 3.2 ms) recorded in the same PASMCs. In conclusion, multiple RyR subtypes are expressed differentially in peripheral and perinuclear RyR-gated Ca^{2+} stores; the molecular complexity and spatial heterogeneity of RyRs may facilitate specific Ca^{2+} regulation of cellular functions in PASMCs.

calcium sparks; ryanodine receptors; calcium signaling; intralobar pulmonary arteries; perinuclear sarcoplasmic reticulum

INTRACELLULAR CA^{2+} IS a ubiquitous messenger for numerous cellular functions ranging from gene expression to muscle contraction. Ca^{2+} signals for these diverse biological processes are generated by various specific Ca^{2+} transporters, delivered globally or locally, and decoded by different effectors according to the signal amplitude and frequency (3). In pulmonary vascular smooth muscle, major attention has been focused on the global elevation of $[Ca^{2+}]_i$ because of its role in smooth muscle contraction. However, local Ca^{2+} release events or "Ca^{2+} sparks" have been identified and characterized recently in pulmonary arterial smooth muscle cells (PASMCs) (26, 38, 40, 50, 53). Emerging evidence suggests that Ca^{2+} sparks of PASMCs regulate pulmonary vascular reactivity in a unique manner. In rat intralobar PASMCs, Ca^{2+} sparks are associated with membrane depolarization (40), instead of hyperpolarization reported in systemic vascular myocytes (34). They are activated by endothelin-1 (ET-1) through an ET_A receptor/phospholipase C (PLC)/inositol 1,4,5-trisphosphate (IP_3)-dependent Ca^{2+} signaling pathway, contributing to the ET-1-induced vasoconstriction (53). Moreover, Ca^{2+} sparks are elicited by metabolic inhibition (50) and have been implicated to play central roles in perinatal pulmonary vasodilation and hypoxic pulmonary vasoconstriction (38, 39). Therefore, elucidation of the molecular and cellular basis of Ca^{2+} spark is important for understanding the regulation of pulmonary circulation.

The Ca^{2+} release channel, ryanodine receptor (RyR), is the mediator of Ca^{2+} sparks. Three different RyR subtypes, namely RyR1, RyR2, and RyR3, were isolated/cloned originally from skeletal muscle, cardiac muscle, and brain, respectively (21, 36, 48). Four RyR monomers of each subtype tetramerize to form an RyR-sensitive Ca^{2+} release channel, and clustering of 10–100 of these channels on the sarcoplasmic reticulum (SR) forms a release unit for Ca^{2+} spark generation (15, 16). In some tissues, such as skeletal and cardiac muscles, a specific RyR subtype is preferentially expressed. However, expression of multiple RyR subtypes is common in many other tissues. In rat aorta, mesenteric arteries, cerebral arteries, portal veins, and porcine coronary arteries, coexpression of all three RyR subtypes has been reported (6, 32, 35, 49). Evidence suggests that RyR1 and RyR2 are required for Ca^{2+} spark generation in these vascular myocytes, whereas RyR3 participates in global Ca^{2+} responses induced by agonists and/or in the modulation of Ca^{2+} spark frequency (6, 32, 33).

In addition to the differences in RyR subtypes, spatial and functional heterogeneities of RyR-gated Ca^{2+} stores have been reported in vascular smooth muscles. Confocal imaging and electron microscopy have shown that RyRs are localized to peripheral junctional SR and to the central nonjunctional SR (30). In the peripheral sarcolemma-SR junctions of cerebral arteries, RyRs are closely associated with L-type Ca^{2+} channels and Ca^{2+}-activated potassium (K_{Ca}) channels to operate as

Address for reprint requests and other correspondence: J. S. K. Sham, Div. of Pulmonary and Critical Care Medicine, Johns Hopkins Asthma and Allergy Center, 5501 Hopkins Bayview Cir., Baltimore, MD 21224 (e-mail: jsks@welchlink.welch.jhu.edu).

The costs of publication of this article were defrayed in part by the payment of page charges. The article must therefore be hereby marked "*advertisement*" in accordance with 18 U.S.C. Section 1734 solely to indicate this fact.

Table 1. *Primers for conventional and real-time RT-PCR experiments*

Gene	Accession Number	Primer	Sequence 5′-3′	Nucleotide Position	Predicted Size, bp
Rat RyR1	XM_341818	sense	5′-GAAGGTTCTGGACAAACACGGG-3′	2085–2106	435
		antisense	5′-TCGCTCTTGTTGTAGAATTTGCGG-3′	2496–2519	
		sense*	5′-AGACAGAGCACACCGGTCAG-3′	2918–2937	83
		antisense*	5′-ACAGTCTCCAGCAGGGAAGA-3′	2981–3000	
Mouse RyR2	NM_023868	sense	5′-GAATCAGCGAGTTACTGGGCATGG-3′	13994–14017	635
		antisense	5′-TTGATCTCTGAGTTCTCCAAAAGC-3′	14605–14628	
		sense*	5′-GGAAGAAAATGAAGCGGAAA-3′	10346–10365	104
		antisense*	5′-AGGGGCACAGATGTTCAGTC-3′	10432–10449	
Rat RyR3	XM_342491	sense	5′-AGAAGAGGCCAAAGCAGAGG-3′	8310–8329	269
		antisense	5′-GGAGGCCAACAGTCAGA-3′	8562–8578	
		sense*	5′-CCCTGCTCAGAAGGATGAAGG-3′	2607–2626	115
		antisense*	5′-AACCAGTGGGAGGAGAACCT-3′	2702–2721	
Rat β-actin	BC063166	sense*	5′-TCTGTGTGGATTGGTGGCTCTA-3′	1093–1114	69
		antisense*	5′-CTGCTTGCTGATCCACATCTG-3′	1141–1161	

RyR, ryanodine receptor. *Primers used in real-time PCR.

a functional unit (25, 31), such that Ca^{2+} influx via L-type Ca^{2+} channel triggers RyRs to generate Ca^{2+} sparks, which activate nearby K_{Ca} channels, causing membrane hyperpolarization to negatively feedback regulate L-type Ca^{2+} channels (23). In rat portal veins, RyRs reside in a well-developed superficial network of SR (20). However, most of the Ca^{2+} sparks in these cells are generated from only one major frequent discharge site (FDS) located on a prominent portion of SR close to the nuclear envelope. This unique spatial location of FDS may signify specific physiological functions other than membrane potential regulation.

Besides all these studies in systemic vascular myocytes, similar information on RyRs and RyR-gated Ca^{2+} stores in PASMCs is unavailable. In the present study, we sought to identify and quantify the relative expression of RyR subtypes, to determine the spatial distribution of RyR subtypes, and to characterize the functional activity of RyR-gated Ca^{2+} stores in PASMCs.

MATERIALS AND METHODS

Isolation and culture of PASMCs. PASMCs were enzymatically isolated and transiently cultured as previously described (45). In brief, male Wistar rats (150–250 g) were injected with heparin and anesthetized with pentobarbital sodium (130 mg/kg ip). They were exsanguinated, and lungs were removed and transferred to a petri dish filled with HEPES-buffered salt solution (HBSS) containing (in mM) 130 NaCl, 5 KCl, 1.2 $MgCl_2$, 1.5 $CaCl_2$, 10 HEPES, and 10 glucose, pH 7.4 (adjusted with NaOH). Second- and third-generation intrapulmonary arteries (~300–800 μm) were isolated and cleaned free of connective tissue. The endothelium was removed by gently rubbing the luminal surface with a cotton swab. Arteries were then allowed to recover for 30 min in cold (4°C) HBSS, followed by 20 min in reduced-Ca^{2+} (20 μM) HBSS at room temperature. The tissue was digested at 37°C for 20 min in 20 μM Ca^{2+} HBSS containing collagenase (type I, 1,750 U/ml), papain (9.5 U/ml), bovine serum albumin (BSA, 2 mg/ml), and dithiothreitol (1 mM), then removed, and washed with Ca^{2+}-free HBSS to stop digestion. Single smooth muscle cells were gently dispersed by trituration with a small-bore pipette in Ca^{2+}-free HBSS at room temperature. The cell suspension was then placed on 25-mm glass coverslips and transiently (16–24 h) cultured in Ham's F-12 medium (with L-glutamine) supplemented with 0.5% fetal calf serum (FCS), 100 U/ml streptomycin, and 0.1 mg/ml penicillin.

RT-PCR. Total RNA was isolated from deendothelialized rat intralobar pulmonary arteries (PAs) and aorta with TRIzol reagent (Invitrogen, Carlsbad, CA) according to the manufacturer's protocol. Genomic DNA contamination was removed by DNA-free DNase Treatment and Removal Reagents (Ambion, Austin, TX). In brief, 2 units of DNase I were added to the isolated RNA and incubated for 30 min at 37°C. Then, DNase Inactivation Reagent was added and incubated for 2 min at room temperature. The samples were centrifuged at 10,000 *g* for 1 min to pellet the DNase Inactivation Reagent. The supernatants were collected, and the amounts of RNA were determined by measuring the optical density at 260 nm. Total RNA was also isolated from skeletal muscle, heart, and brain as positive controls for RyR1, RyR2, and RyR3, respectively. We used 2 μg of total RNA for first-strand cDNA synthesis with random hexamer primers and Superscript II RNase H^- Reverse Transcriptase (Invitrogen, Carlsbad, CA). The resulting first-strand cDNAs were directly used as templates for PCR amplification. Sense and anti-sense primers specific for RyR1, RyR2, or RyR3, as listed in Table 1 were used. Reactions were carried out using PCR SuperMix (GIBCO-BRL) with the following parameters: denaturation at 94°C for 30 s, annealing at 56–60°C for 30 s, and extension at 68°C for 45 s. A total of 30 cycles were performed. This was followed by a final extension at 72°C for 10 min and then stored at 4°C. PCR products were analyzed by 1.2% agarose gel electrophoresis and visualized by staining with ethidium bromide. Parallel reactions were run for each RNA sample in the absence of Superscript II to access the degree of genomic DNA contamination.

Quantitative real-time RT-PCR. We used 2 μl of cDNA as the template in each 25-μl PCR reaction with SYBR Green Core PCR reagent (PE Applied Biosystem). The specific primers as listed in Table 1 were used. Cycling conditions were: initial enzyme inactivation at 95°C for 10 min, followed by 40 cycles at 95°C for 15 s, 60°C for 30 s, and 72°C for 30 s. All cycling reactions were performed in the presence of 3 mM $MgCl_2$. PCR assays were performed with the Applied Biosystems PRISM 7700 Sequences Detect System. All PCR data were captured using Sequence Detector Software (SDS version 1.6, PE Applied Biosystem). Using the same protocol, we generated standard curves from serial dilutions of purified PCR products, which allowed quantitation of the specific mRNA of interest. The threshold cycle value for each sample was used to calculate the initial quantity of cDNA template by the standard curve method. We also normalized data from each sample by dividing the quantity of target gene cDNA by the quantity of β-actin cDNA to correct for variability in individual samples. We ran parallel reactions using each RNA sample as tem-

plate to assess the degree of contaminating genomic DNA. Negative control reactions without template were also performed.

Western blotting. Deendothelialized PAs and aorta were homogenized in buffer containing 20 mM imidazole (pH 7.0), 0.3 M sucrose, and 1% protease inhibitor cocktail. The homogenate was centrifuged at 4°C with 500 *g* for 2 min to remove the debris. The supernatant was stored at −80°C before use. The protein concentration was estimated by the bicinchoninic acid method, using BSA as standard. Protein samples (20 μg) were resolved in an 8% SDS-PAGE gel and electrotransferred to a nitrocellulose membrane (Schleicher & Schuell). The membrane was blocked with 3% (wt/vol) nonfat dry milk in PBS containing 0.02% Tween 20 (PBST) for 1 h at room temperature, followed by incubation with polyclonal antibodies against RyR1, RyR2, or RyR3 antibodies (from Dr. Sidney Fleischer's laboratory) at 1:500 dilution in blocking solution overnight at 4°C. Antibodies of RyR1 (Upstate Biotechnology, Lake Placid, NY), RyR2 (Affinity Bioreagents, Golden, CO), and RyR3 (gift from Dr. Gerhard Meissner) were also used for comparison. Nitrocellulose membrane was then washed with PBST. After being washed, the membrane was incubated with horseradish peroxidase-conjugated secondary antibody (Amersham) at 1:3,000 dilution at room temperature for 2 h. Excess secondary antibody was again washed, and the bound secondary antibody was detected with enhance chemiluminescence (Western Lightning Chemiluminescence Reagent Plus; Perkin-Elmer Life Science Products, Boston, MA) according to the manufacturer's protocols. Rat skeletal muscle, heart, and brain membrane proteins were used as positive controls.

Immunolocalization of RyR subtypes. PASMCs were fixed in 2% paraformaldehyde for 20 min. The cells were washed with 0.75% glycine in PBS for 30 min, followed by permeabilization with 0.05% Triton X-100 for 30 min. The cells were then incubated with unconjugated donkey anti-rabbit or anti-mouse secondary antibodies (20 μg/ml) to block nonspecific binding for 2 h and then incubated overnight with isoform-specific anti-RyR antibodies. Primary antibodies included mouse monoclonal IgM anti-RyR type I (20 μg/ml, Upstate Biotechnology), mouse monoclonal IgG anti-RyR type II (10 μg/ml, Affinity Bioreagents), and rabbit polyclonal anti-RyR type III (5 μg/ml, from Dr. Sidney Fleischer's laboratory). Antibody-specific binding was visualized with either donkey CY2-conjugated or CY5-conjugated secondary antibodies (3 μg/ml, Jackson ImmunoResearch), which were affinity purified for multiple labeling. BSA (2%) and Triton X-100 (0.05%) were included in PBS for antibody dilution. Incubation was carried out in a moistened chamber at 4°C. Immunolocalization was examined with an MRC-1000 confocal scanning unit (Bio-Rad) equipped with a krypton-argon laser, and images were acquired with a Zeiss plan-apochromat objective [×40, numerical aperture (NA) = 1.2]. PASMCs without exposure to primary antibodies were used as a negative control. Two-dimensional fluorescent images were deconvoluted with SimplePCI software (Compix, Cranberry Township, PA).

Confocal imaging and measurement of Ca^{2+} sparks. BODIPY TR-X ryanodine and Fluo-5N were used for localization of RyRs and SRs in freshly isolated PASMCs according to Gordienko et al. (20) and Shannon et al. (44), respectively. RyRs were stained by incubation of PASMCs with 1 μM BODIPY TR-X ryanodine for 15 min, and SR was loaded with 10 μM Fluo-5N AM (Molecular Probes) for 2 h, and then 1.5 h was allowed for deesterification and outward leak of cytosolic indicator all at 37°C. Confocal images were acquired under a Zeiss LSM-510 inverted confocal microscope (Carl Zeiss) with a Zeiss Plan-Neofluor ×40 oil immersion objective (NA = 1.3). BODIPY TR-X was excited by the 543 nm line of an HeNe laser, and the emitted fluorescence signal was captured at wavelength >585; Fluo-5N was excited by the 488-nm line of an argon laser, and the emission was detected at 505–550 nm. Ca^{2+} sparks were visualized as previously described (40) with the membrane-permeable Ca^{2+}-sensitive fluorescent dye fluo-3 acetoxymethyl ester (fluo-3 AM). PASMCs were loaded with 5–10 μM fluo-3 AM (dissolved in DMSO with 20% pluronic acid) for 30–45 min at room temperature (~22°C) in normal Tyrode solution containing (in mM) 137 NaCl, 5.4 KCl, 2 $CaCl_2$, 1 $MgCl_2$, 10 HEPES, and 10 glucose, pH 7.4 (adjusted with NaOH). Cells were washed thoroughly with Tyrode solution to remove extracellular fluo-3 AM and rested for 15–30 min in a cell chamber to allow complete deesterification of cytosolic dye. Fluo-3 AM was excited at 488 nm, and fluorescence was measured at >505 nm. Confocal pinhole was set to render a spatial resolution of 0.4 μm in the *x*-*y*-axis and 0.8 μm in the *z*-axis. Two-dimensional images were scanned at 0.075 μm/pixel, 512 pixels/line, 256 lines/image once every 0.5 s. Line-scan images were collected at 0.075 μm/pixel, 512 pixels/line at 2-ms intervals for 512 lines/image once every 10 s. We minimized photobleaching and laser damage to the cells by attenuating the laser to ~1% of its maximum power (25 mW) with an acousto-optical tunable filter. Cells that did not respond to an external solution containing 10 mM Ca^{2+} and 0.5 mM caffeine applied at the end of experiments were discarded. All experiments were performed at room temperature. Images were processed with custom-written algorithms using the IDL software package. Ca^{2+} sparks were analyzed as described previously (40, 53).

RESULTS

Identification of RyR subtypes in PASMCs. Expression of RyR subtypes in pulmonary arterial smooth muscle was first identified using conventional RT-PCR. Figure 1*A* shows the RT-PCR products amplified from mRNA isolated from deendothelialized intralobar PAs. mRNA of all three RyR subtypes were clearly detected after 30 cycles. PCR amplified products of RyR1, RyR2, and RyR3 were consistent with the predicted sizes and matched with the positive controls generated from skeletal muscle, heart, and brain, respectively. The expression of RyR proteins in intralobar PAs was examined by Western blot. Specific antibodies against RyR1, RyR2, and RyR3 detected clear bands of protein with molecular mass >400 kDa from skeletal muscle, heart, and brain, respectively. Matched protein bands of all three RyR subtypes were detected in samples of intralobar PAs (Fig. 1, *C* and *D*). Similar results were obtained in deendothelialized aorta smooth muscle (Fig. 1, *B* and *E*), suggesting that multiple RyR subtypes are coexpressed in both pulmonary and systemic vascular smooth muscle.

The relative expressions of three RyR subtype mRNA in PAs and aorta were determined by quantitative real-time RT-PCR. The amplification curves of RyR1, RyR2, RyR3, and β-actin are shown in Fig. 2. Amplification efficiencies of the three RyR subtypes were similar according to our specific primers and PCR conditions, with slopes of the standard curves ranging between −3.525 and −3.663. RyR2 mRNA was most abundant among the three RyR subtypes in PAs. The amount of RyR2 mRNA, quantified by normalization with β-actin as the internal control, was equivalent to 0.25 ± 0.04% of β-actin. It was ~15–20 times more abundant than RyR1 and RyR3, which were equivalent to 0.011 ± 0.002 and 0.017 ± 0.004% of β-actin, respectively. The expressions of RyR subtypes in aortic smooth muscle were similar to that in pulmonary arterial smooth muscle. The normalized amounts of RyR1, RyR2, and RyR3 mRNA in aorta were 0.019 ± 0.011, 0.236 ± 0.065, and 0.011 ± 0.003%, respectively.

Localization of RyRs in PASMCs. The subcellular distribution of RyR in PASMCs was visualized by staining the myocytes with the cell-permeable fluorescent probe BODIPY TR-X ryanodine. In serum-starved transiently cultured (0.5%

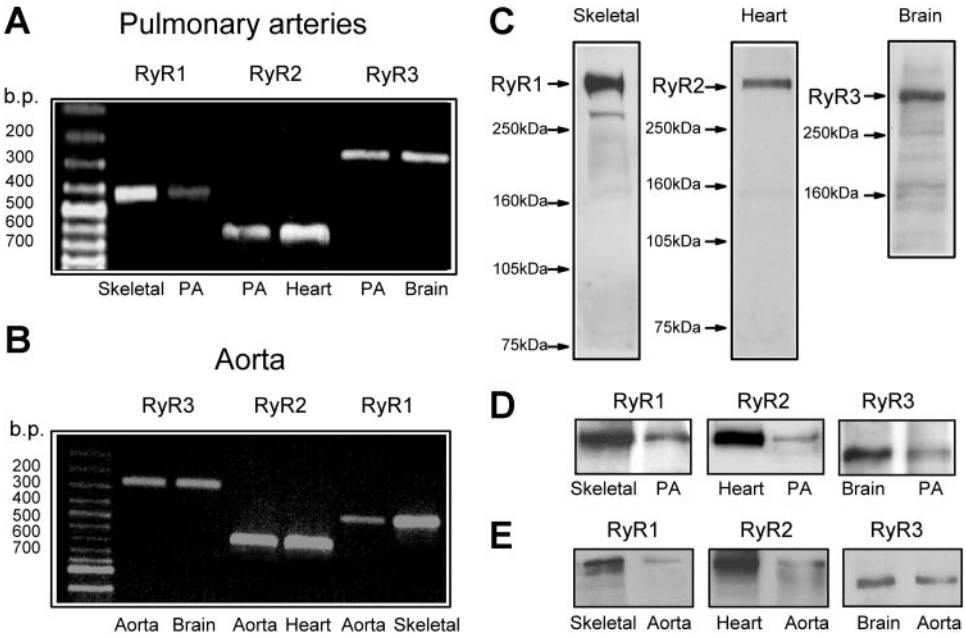

Fig. 1. RT-PCR analysis of ryanodine receptor (RyR) subtypes in rat intralobar pulmonary arteries (PAs, *A*) and aorta (*B*). Skeletal muscle, heart, and brain mRNAs and proteins were used as positive control for RyR1, RyR2, and RyR3, respectively. The predicted sizes of the PCR products were 435 bp for RyR1, 635 bp for RyR2, and 269 bp for RyR3. mRNAs for all 3 RyR subtypes were expressed in both intralobar PAs and aorta. *C*: immunoblots showing strong signals of RyR1, RyR2, and RyR3 subtypes in the positive control samples from skeletal muscle, heart, and brain, respectively. Immunoblot analysis of RyR1, RyR2, and RyR3 in PAs (*D*) and aorta (*E*), respectively.

FCS, 16–24 h) PASMCs, confocal imaging revealed a pattern of interconnecting pockets of RyRs that were especially well developed in the subsarcoplasmic and perinuclear regions (Fig. 3*A*). Three-dimensional reconstruction of the BODIPY TR-X ryanodine-stained PASMC images showed that RyRs in the cytoplasmic regions were located in close association with the sarcolemma, with minor staining in the inner cytosol along the longitudinal axis. In contrast, RyRs in the perinuclear region resided in massive structures around the nucleus and occupying most of the central region of the myocytes except the interior of the nucleus.

The distribution of SR was visualized with the low-affinity Ca^{2+} fluorescent dye Fluo-5N AM according to Shannon et al. (44). This technique makes use of the property that the dye fluoresces only when it is bound at high [Ca^{2+}] in the SR (>300 μM) but does not fluoresce at low [Ca^{2+}] (~100 nM) in the cytosol or mitochondria. Figure 3*B* shows that SRs in PASMCs exhibited similar peripheral and perinuclear patterns. Costaining of PASMCs with BODIPY TR-X ryanodine and Fluo-5N showed clear colocalization of RyRs in peripheral and perinuclear SRs, indicating that RyRs are indeed present in the SRs of the two regions.

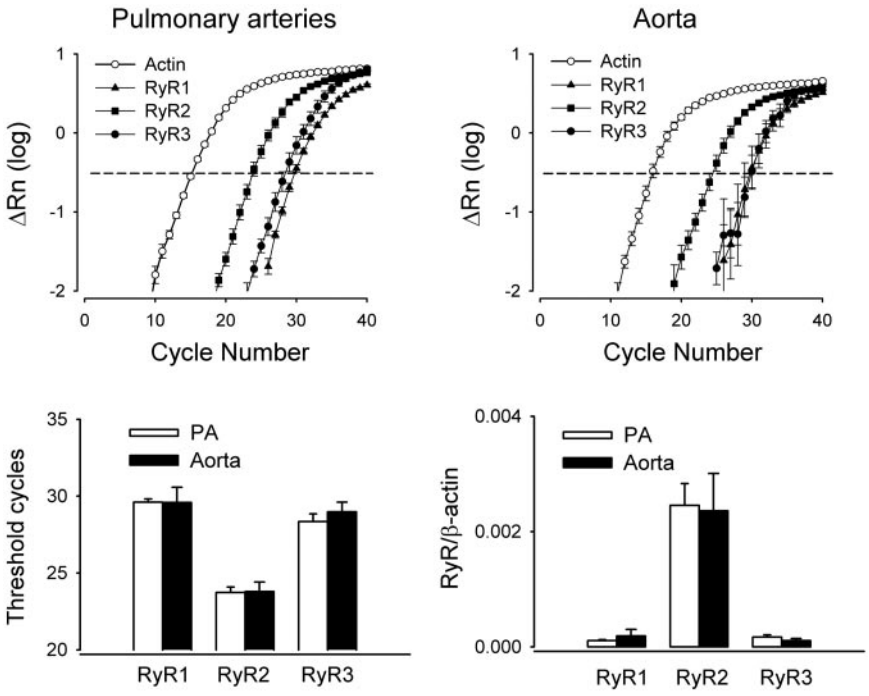

Fig. 2. Real-time RT-PCR analysis of the relative expression of RyR mRNA in rat intralobar PAs and aorta using β-actin as the internal standard. *Top*: amplification curves of β-actin, RyR1, RyR2, and RyR3 of intralobar PAs (*left*) and aorta (*right*). Rn, normalized reporter signal. *Bottom*: threshold cycles (*left*) and the normalized amount of RyR subtype mRNA (*right*) in PAs and aorta. The amounts of mRNA of RyR1, RyR2, and RYR3 expressed in PAs and aorta were not statistically different. We used 5 animals for each preparation.

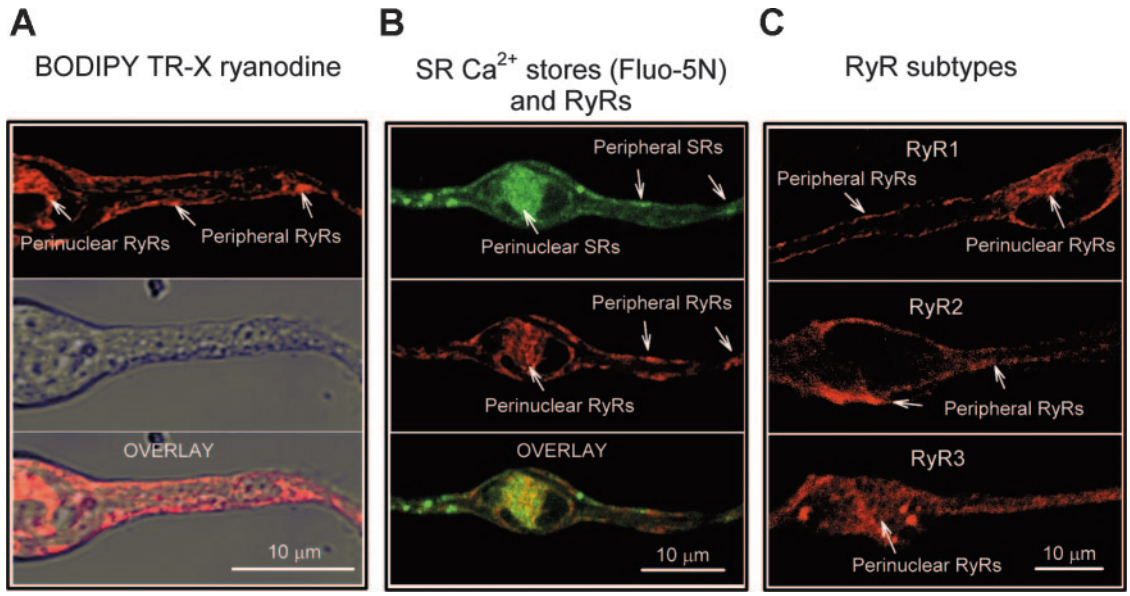

Fig. 3. Localization of RyRs in pulmonary arterial smooth muscle cells (PASMCs). *A*: fluorescent-staining of RyRs using BODIPY TR-X ryanodine (*top*), showing discrete patches of RyRs in cell periphery close to the sarcolemmal membrane and large aggregations of RyRs in the perinuclear region. Transmitted light image (*middle*) and the overlay image (*bottom*). *B*: costaining of RyRs using BODIPY TR-X ryanodine (*top*) and SR Fluo-5N (*middle*) in a PASMC. *Bottom*: overlay of the images showing that colocalization of RyRs and sarcoplasmic reticula (SRs, yellow color) in the peripheral and perinuclear regions. *C*: immunostaining of RyR1 (*top*), RyR2 (*middle*), and RyR3 (*bottom*) using RyR subtype-specific antibodies in PASMCs. Arrows indicate either RyR or SR sites.

To further examine the subcellular localization of RyR subtypes in PASMCs, we immunostained individual RyR subtypes using specific antibodies (Fig. 3*C*). High-resolution deconvoluted confocal images showed strong immunofluorescent signals of RyR1 in both the peripheral and perinuclear regions, similar to the patterns of BODIY TR-X ryanodine and Fluo-5N. Clear immunostaining for RyR2 was also observed in the peripheral/subsarcolemmal sites, but with much weaker signals in the perinuclear region. In contrast, RyR3s were detected diffusely in the perinuclear region and the cytosol without a clear subsarcoplasmic affiliation. These results suggest that the three RyR subtypes may localize differentially in different populations of SR.

Generation of Ca^{2+} sparks from peripheral and perinuclear RyR-gated Ca^{2+} stores. The functional activity of RyRs in peripheral and perinuclear SR was examined by recording Ca^{2+} sparks with 100 sequential two-dimensional confocal scans for each cell (Fig. 4). Under control conditions, Ca^{2+} spark frequency was very low, averaging 0.014 ± 0.003 spark·μm^{-2}·100 frames^{-1} (Fig. 5*A*). Spark frequencies recorded from peripheral and perinuclear sites (within 3 μm around the nuclear region) were similar, 0.016 ± 0.04 and

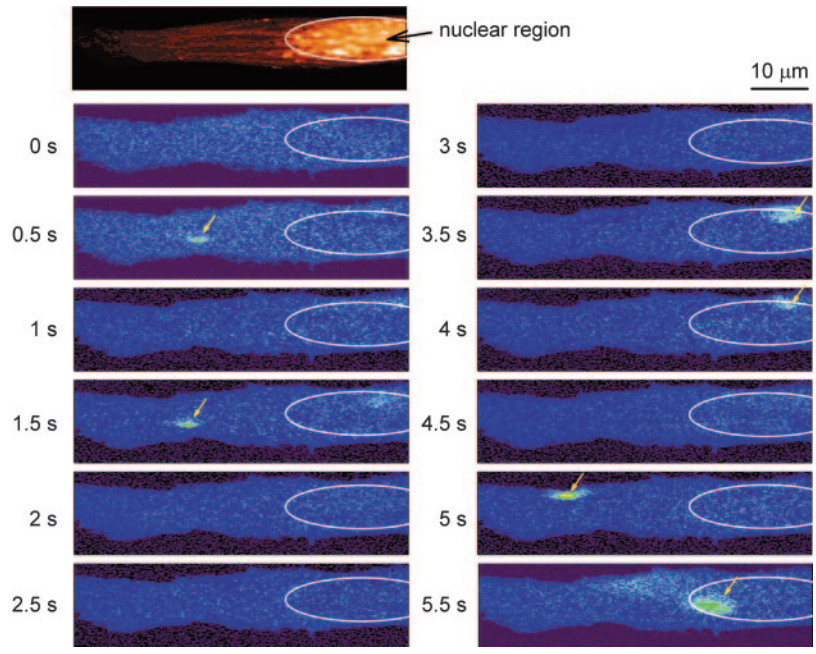

Fig. 4. Sequential images of PASMC showing Ca^{2+} sparks occurred in peripheral and perinuclear sites in the presence of 0.5 mM caffeine and 10 mM Ca^{2+}. *Top left*: raw image with the characteristically strong Fluo-3 fluorescence in the perinuclear region; remaining panels are fluorescence images after background subtraction and baseline normalization. The white elliptical line indicates the perinuclear region, and the arrows indicate the sites of Ca^{2+} spark generation.

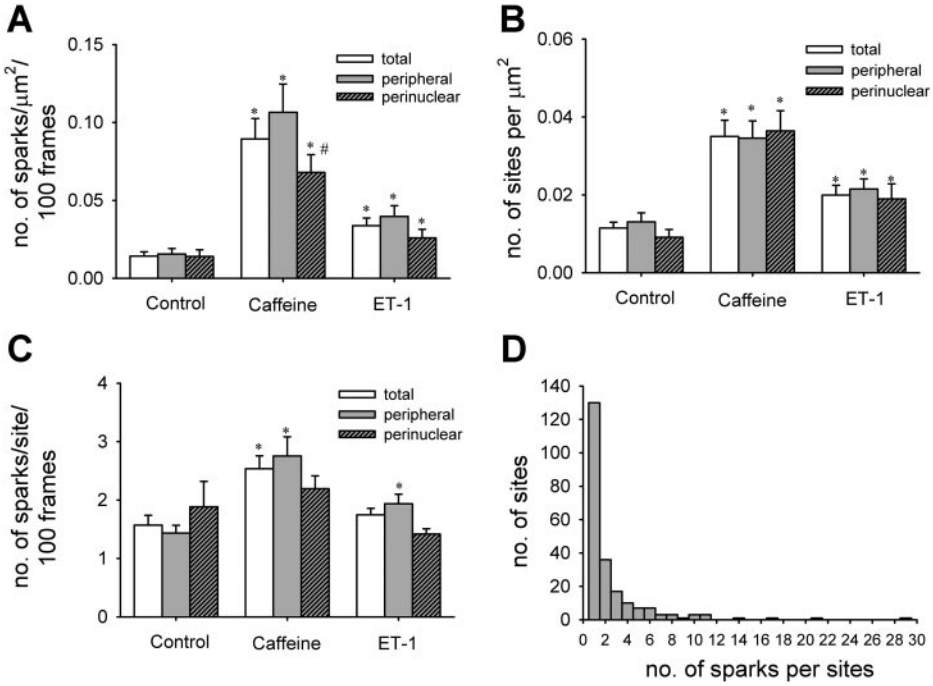

Fig. 5. Analysis of Ca^{2+} sparks generated from the peripheral and perinuclear sites. *A*: total spark frequency and spark frequency of peripheral and perinuclear sites under control condition or in the presence of 0.5 mM caffeine or 0.3 nM endothelin (ET)-1. *B*: total number of sites and the number of peripheral and perinuclear sites recorded under control condition or in the presence of 0.5 mM caffeine or 0.3 nM ET-1. *C*: averaged number of sparks per sites detected under control condition or in the presence of 0.5 mM caffeine or 0.3 nM ET-1. *D*: frequency distribution of number of sparks generating in each site. *Significant difference from control. #Significant difference from perinuclear sites.

0.014 ± 0.003 spark·μm^{-2}·100 $frames^{-1}$ ($n = 27$ cells), respectively. Maximal enhancement of Ca^{2+} spark using 0.5 mM caffeine plus 10 mM Ca^{2+} increased whole cell spark frequency to 0.090 ± 0.013 spark·μm^{-2}·100 $frames^{-1}$ ($n = 21$ cells, $P < 0.05$), with greater enhancement of Ca^{2+} sparks generated in the peripheral (0.107 ± 0.018 spark·μm^{-2}·100 $frames^{-1}$) than the perinuclear (0.068 ± 0.012 spark·μm^{-2}·100 $frames^{-1}$) sites. Moreover, the vasoconstrictor ET-1 (0.3 nM) caused significant activation of Ca^{2+} spark at both the peripheral (0.040 ± 0.007 spark·μm^{-2}·100 $frames^{-1}$, $n = 38$ cells) and perinuclear sites (0.026 ± 0.005 spark·μm^{-2}·100 $frames^{-1}$, $n = 38$ cells), suggesting that ET-1 can regulate the activity of the two populations of RyRs.

To further examine the spatial distribution of Ca^{2+} sparks in individual PASMC, the location of each Ca^{2+} spark in a PASMC was registered. Ca^{2+} sparks recorded within a radius of 2 μm, which is approximately equivalent to the size or full-width-half-maximum (FWHM) of a Ca^{2+} spark, were considered as Ca^{2+} release from the same site. Data were analyzed to determine the number of sites per cell and the number of Ca^{2+} sparks generated per site in every 100 two-dimensional scans (Fig. 5, *B* and *C*). In control PASMCs, there were 0.012 ± 0.002 spark-generating sites per μm^2, and most of these sites fired only once or twice during the recording period. The number of sites was increased significantly in PASMCs stimulated by caffeine (0.035 ± 0.004 sites/μm^2, $P < 0.05$) or by ET-1 (0.020 ± 0.002 sites/μm^2, $P < 0.05$), and the increase was similar in the peripheral and perinuclear regions (Fig. 5*B*). By contrast, the averaged number of spark per site was increased only moderately in caffeine-treated PASMCs, from a control value of 1.57 ± 0.17 to 2.54 ± 0.22 spark·$site^{-1}$·100 $frames^{-1}$ ($P < 0.05$), with the increase occurring mainly in the peripheral sites. Frequency distribution analysis (Fig. 5*D*) shows that 74% of these sites fired only one or two times in the 100 frames recorded; therefore, most of these sites appear to be random/stochastic in nature, even when the spark occurrence was maximally activated by caffeine and extracellular Ca^{2+}. However, 10% of the sites fired more than five times during the two-dimensional scanning period. These "hot spots" were not confined to a specific region, i.e., could be either peripheral or perinuclear, and other less-active sites were usually observed in the same cell. Occasionally, frequent spark activity escalated to initiate regional elevation of $[Ca^{2+}]_i$ and propagating Ca^{2+} waves (Fig. 6).

Kinetics of peripheral and perinuclear Ca^{2+} sparks. The spatial-temporal characteristics of peripheral and perinuclear sparks were examined under the line-scan mode (Fig. 7). Ca^{2+} sparks originated from the peripheral sites had the typical fast activating and inactivating kinetics. The averaged amplitude [change in fluorescence (ΔF)/resting fluorescence (F_0)], duration [full-duration/half-maximum (FDHM)], and width/size (FWHM) of the peripheral sparks were 0.74 ± 0.03, 44.6 ± 3.2 ms, and 1.65 ± 0.09 μm ($n = 105$ sparks from 40 cells), respectively, similar to our previous studies (40, 53). In comparison, the averaged amplitude and the size of the perinuclear sparks were similar with $\Delta F/F_0 = 0.75 \pm 0.03$ and FWHM = 1.7 ± 0.08 μm ($n = 97$ sparks from 40 cells). However, the duration of perinuclear sparks was significantly longer (FDHM = 71.2 ± 7.5 ms, $P < 0.001$). Further examination of individual Ca^{2+} sparks showed that the perinuclear sparks could be divided into the short-duration Ca^{2+} sparks, which resembled the typical Ca^{2+} sparks of the peripheral sites, and the prolonged Ca^{2+} sparks, which lasted for several hundred milliseconds (FDHM: short sparks = 43.37 ± 2.56 ms; long sparks = 193.3 ± 22.6 ms, $P < 0.001$). The latter accounted for ~18% (17 out of 97) of all perinuclear sparks. Figure 8 contrasts the kinetic differences between the peripheral Ca^{2+} sparks, the short-duration, and the prolonged perinuclear Ca^{2+} sparks. Typically, the prolonged perinuclear Ca^{2+} sparks had a maintained plateau following the initial rise in $[Ca^{2+}]$ and might occur repeatedly at the same site. Moreover, the prolonged sparks had significantly higher amplitude and larger

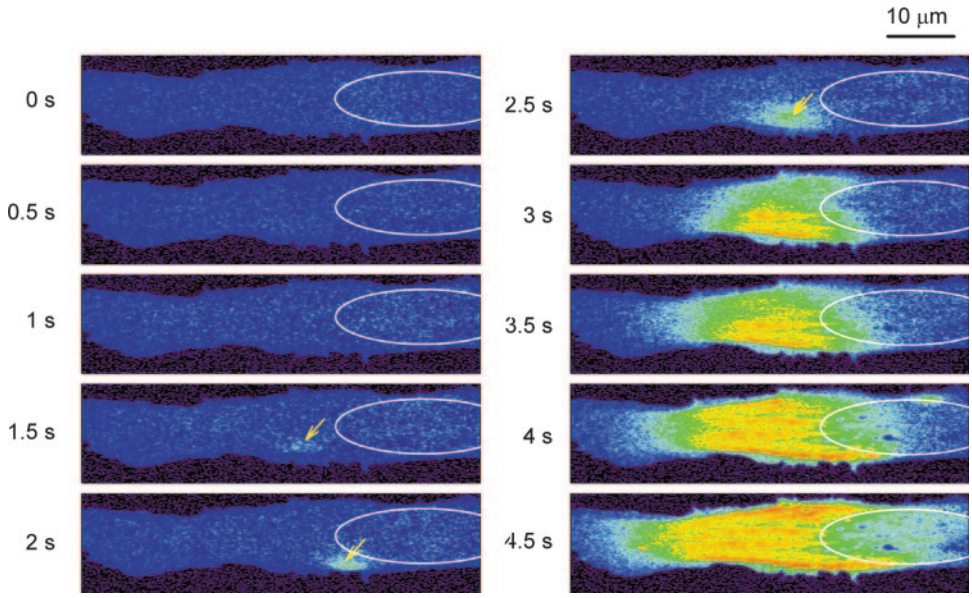

Fig. 6. Initiation of global Ca^{2+} transient from a local Ca^{2+} "hot spot" in the presence of 0.5 mM caffeine and 10 mM Ca^{2+}. Sequential images showing localized Ca^{2+} sparks occurred at a site before global Ca^{2+} increase in the cytoplasm. Ca^{2+} release propagated from the frequent sparking site to the rest of the cytoplasm. Ca^{2+} increase in the nuclear region was apparently less compared with the cytoplasm. The white elliptical line indicates the nuclear region, and the arrows indicate the sites of Ca^{2+} wave initiation.

size than the short-duration perinuclear or peripheral sparks. The heterogeneities in the temporal and spatial properties suggest major differences in the gating mechanism of perinuclear Ca^{2+} sparks.

DISCUSSION

In the present study, we have for the first time characterized the relative expression of RyR subtypes, determined the spatial distributions of RyR subtypes and RyR-gated Ca^{2+} stores, and compared the regional differences in the spatial and temporal properties of Ca^{2+} sparks in rat intralobar PASMCs. Our results show that *1*) mRNAs and proteins of all three RyR subtypes are expressed in rat intralobar PASMCs, with RyR2 mRNA being most abundantly transcribed; *2*) RyRs are localized in the subsarcolemmal and the perinuclear regions, but the distributions of various RyR subtypes in these regions are different; *3*) RyR-gated stores in the two regions are capable of generating Ca^{2+} sparks, and their activities are regulated by the agonists ET-1 and caffeine; and *4*) a subpopulation of Ca^{2+} sparks originate from the perinuclear region exhibit prolonged duration, higher amplitude, and larger spatial spread, distinguishing themselves from the typical fast transient Ca^{2+} sparks recorded in the peripheral and perinuclear sites. These findings provide information on the molecular and subcellular complexity of Ca^{2+} signaling in PASMCs and raised the intriguing possibility that Ca^{2+} sparks generated from different regions may participate in different cellular functions.

Coexpression of all three RyR subtypes in pulmonary arterial smooth muscle is clearly demonstrated at both mRNA and protein levels by conventional RT-PCR, quantitative real-time RT-PCR, Western blot analysis, and immunostaining. The expression profiles of RyR mRNA are similar in rat PAs and aorta, with RyR2 being the major RyR gene transcribed. However, because strong signals of RyR1 and RyR3 proteins were observed in both immunoblots and immunostainings, it is possible that the efficiencies of protein translation may be higher for RyR1 and RyR3 in PASMCs. Previous studies show that different RyR subtypes might mediate different physiological functions in vascular smooth muscle cells. Suppression of either RyR1 or RyR2 in portal vein myocytes using antisense oligonucleotides blocked the increase in Ca^{2+} spark induced by depolarization or by elevation of extracellular $[Ca^{2+}]$, whereas suppression of RyR3 had no effect on spontaneous spark frequency but attenuated caffeine- or phenyleph-

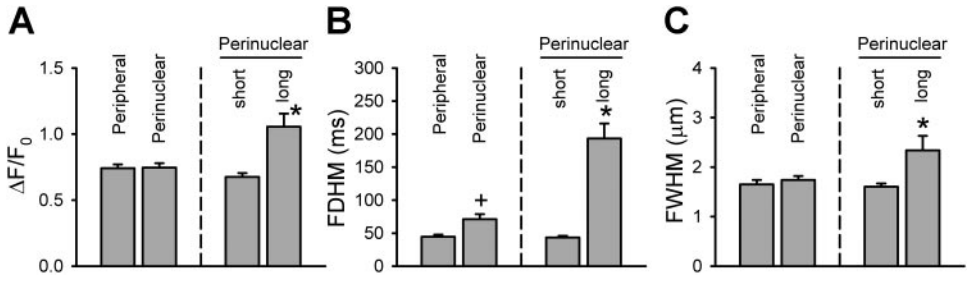

Fig. 7. Spatial and temporal characteristics of Ca^{2+} sparks generated from peripheral and perinuclear sites. *A*: averaged amplitude of Ca^{2+} sparks generated from the peripheral and perinuclear regions (*left* bars), and the amplitudes of the short and prolonged perinuclear Ca^{2+} sparks (*right* bars). *B*: averaged duration [full duration/half-maximum (FDHM)] of Ca^{2+} sparks generated from the peripheral and perinuclear regions (*left* bars), and the durations of the short and prolonged perinuclear Ca^{2+} sparks (*right* bars). *C*: averaged size [full width/half-maximum (FWHM)] of Ca^{2+} sparks generated from the peripheral and perinuclear regions (*left* bars), and the size of the short and prolonged perinuclear Ca^{2+} sparks (*right* bars). +Significant difference between peripheral and perinuclear sparks; *significant difference between short and long perinuclear sites. Averaged data were generated from 40 cells.

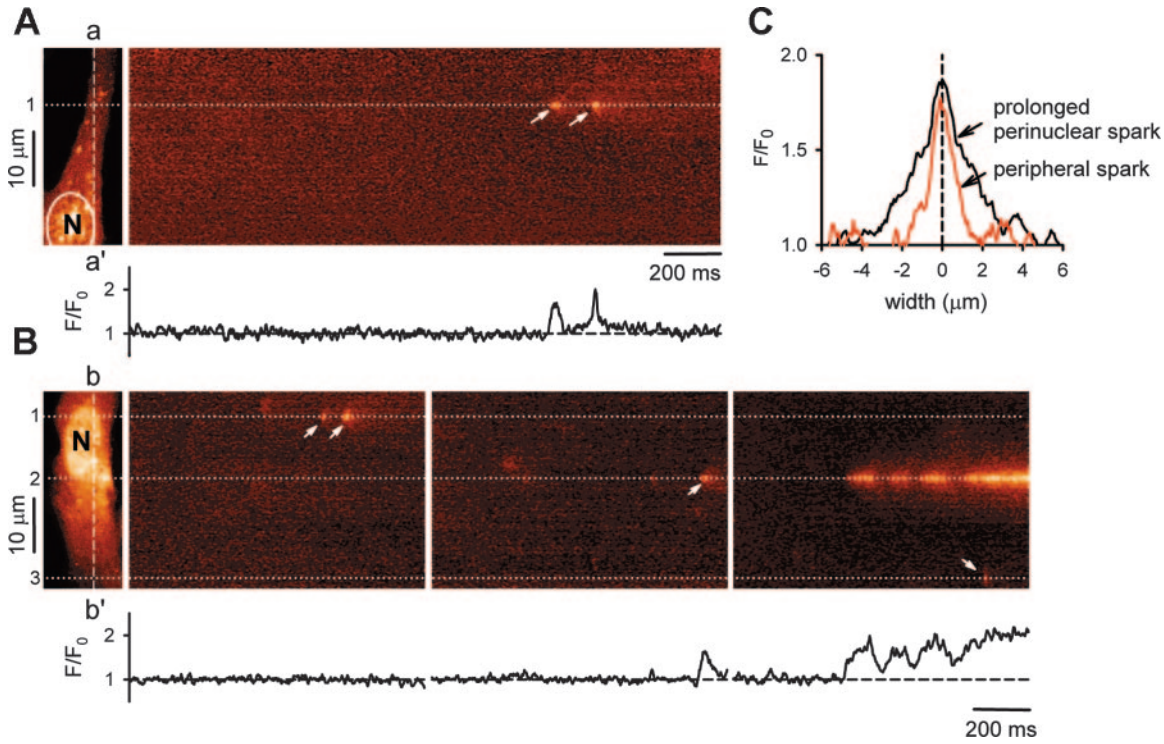

Fig. 8. Line-scan images of Ca^{2+} spark in the peripheral and perinuclear sites. *A*: 2 Ca^{2+} sparks, with typical fast activation and inactivation kinetics, recorded in a peripheral site. The dashed line a-a′ in the 2-dimensional image indicates the position of the scan line. *Bottom*: temporal profile of the fluorescence signal (F/F_0) recorded at *point 1*. *B*: 3 line-scan images showing short and prolonged Ca^{2+} sparks in the perinuclear *sites 1* and *2*. The dashed line b-b′ indicates the position of the scan line. *Bottom*: F/F_0 recorded at *point 2*. A peripheral spark was also recorded at the peripheral *site 3* during the discharge of prolonged perinuclear sparks at *site 2* in the last image. *Arrows*: fast peripheral and perinuclear Ca^{2+} sparks. *C*: spatial profiles of typical peripheral (red line) and prolonged perinuclear Ca^{2+} sparks (black lines). N indicates the position of the nucleus.

rine-induced global Ca^{2+} responses (6, 33). Another study in cerebral arterial myocytes showed that the amplitude, size, and duration of Ca^{2+} sparks were unaltered, but Ca^{2+} spark frequency and the associated spontaneous transient outward currents were significantly increased in the RyR3-deficient myocytes (32). These results suggest that RyR1 and RyR2 are both required for Ca^{2+} spark generation presumably because they participate in the formation of RyR clusters (6), whereas RyR3 plays a modulatory role on spark frequency and/or agonist-induced increase in global $[Ca^{2+}]$ in systemic myocytes (32, 33). The precise roles of the different RyR subtypes for Ca^{2+} signaling in PASMCs need further evaluation.

The most intriguing finding of the present study is the clear heterogeneity in the subcellular distribution of RyRs in PASMCs. BODIPY TR-X ryanodine and Fluo-5N staining revealed two populations of peripheral and perinuclear RyR-gated SRs. Immunostaining experiments using RyR subtype-specific antibodies and high-resolution confocal imaging show that RyR1 are present in both the peripheral and perinuclear sites; RyR2 is located mainly in the peripheral sites, whereas RyR3 resides diffusely in the perinuclear region and the cytosol. These results suggest that SRs in the two subcellular regions maybe gated by RyRs of different subtypes. Because RyR subtypes are functionally different in terms of their sensitivities to Ca^{2+}-induced activation and inactivation, ATP and calmodulin-dependent modulation, and their association with FK506-binding protein isoforms (14), the differential distributions of RyR subtypes may allow specific regulation of the peripheral and perinuclear SRs. Moreover, recent studies in heterologous expression system show that RyR2 forms heterotetramer with either RyR1 or RyR3, and a smooth muscle-specific splice variant of RyR3 can form heteromeric channels with RyR2 and suppress the activities of RyR2 (27, 51). It is possible that heteromerization of different RyR subtypes may occur in various subcellular compartments of native PASMCs.

RyR-gated Ca^{2+} stores present in both peripheral and perinuclear regions suggest that RyRs may involve in more diverse physiological functions. Peripheral RyR-gated SRs in PASMCs are located in the subsarcolemmal region, similar to the junctional SRs described in other vascular and striated myocytes. Juxtaposition of RyR-gated SRs with sarcolemma allows local Ca^{2+} signaling between RyRs and sarcolemmal ion channels. In systemic arteries, RyRs are closely associated with K_{Ca} channels to operate as a functional unit for negative feedback regulation of Ca^{2+} influx via L-type Ca^{2+} channels (23, 25, 31). Ca^{2+} sparks produce a highly localized and large increase in $[Ca^{2+}]$ in microdomains proximal to K_{Ca} channels to mediate hyperpolarization and vasodilation. However, the local Ca^{2+} interactions between RyRs and sarcolemmal ionic channels are different in adult rat intralobar PASMCs. Ca^{2+} sparks elicited by a subthreshold concentration of caffeine cause a small membrane depolarization in PASMCs instead of hyperpolarization (40), and a Ca^{2+} spark activated by metabolic inhibition is associated with prominent spontaneous transient inward currents mediated by Ca^{2+}-activated Cl^- channels (50). Moreover, inhibition of Ca^{2+} sparks with ryanodine attenuates the ET-1-induced vasoconstriction in pulmonary arteries (53). Hence Ca^{2+} sparks appear to associate more

predominantly with the Ca^{2+}-activated Cl^- channels and perhaps other Ca^{2+}-dependent mechanisms in adult rat intralobar PASMCs, overriding the hyperpolarizing influence of K_{Ca} channels, to enhance vasoconstriction through membrane depolarization. However, it has to be mentioned that spontaneous Ca^{2+} release from RyR-gated stores can activate K_{Ca} channels to cause membrane hyperpolarizations in rabbit PASMCs (2, 29), and global release of Ca^{2+} by caffeine at higher concentrations may preferentially activate K_{Ca} channels in PASMCs of conduit arteries or Ca^{2+}-activated Cl^- channels in PASMCs of resistant arteries (2, 46). Hence, the regulation of membrane potential by Ca^{2+} spark may vary depending on species (2, 29), developmental stages (38, 39, 41), and the size of PAs (1, 46). The intricate mechanisms of membrane potential regulation by Ca^{2+} sparks in vascular myocytes have been discussed in detail elsewhere (see reviews Refs. 24, 25).

Peripheral SR junctions may also provide the sites for receptor-mediated signal transduction. It has been documented that membrane receptors colocalize with their signaling molecules and effector molecules, forming signaling complexes in membrane scaffolds or caveolae (13, 42) to facilitate their specific responses. Our previous results showed that ET-1 elicits Ca^{2+} sparks in PASMCs through ET_A receptor-dependent activation of PLC to generate IP_3, which triggers Ca^{2+} release from IP_3 receptors to cross-activate RyRs (53). Interestingly, all components of the signaling complex, including ET_A receptors, heterotrimeric G proteins, PLC, and IP_3 receptors, have been found in caveolae in various cell types (5, 17, 37, 42), and disruption of caveolae in rat tail arteries completely abolished ET-1-induced contraction but only partially inhibited the contractions elicited by 5-hydroxytryptamine and arginine vasopressin and had no effect on K^+-induced vasoconstriction (12). Because ET-1 causes significant enhancement in spark frequency in the peripheral sites, the peripheral sarcolemmal-SR junctions may function as the focal points of signal transduction for Ca^{2+} spark activation in PASMCs.

By contrast, perinuclear SRs are nonjunctional. Ca^{2+} sparks generated from these sites are, therefore, ineffective in regulating membrane potential through local Ca^{2+} interactions with ion channels. However, the close proximity of these RyRs to the nucleus raises the speculation that Ca^{2+} sparks may participate in the regulation of gene expression. Ca^{2+} ions can effectively modulate gene expression through Ca^{2+}-sensitive transcription factors, such as NF-κB, JNK, nuclear factor of activated T cells (NFAT), cAMP response element binding protein, and myocyte enhancer factor-2 (8–11). A recent study in cerebral arteries shows that Ca^{2+} sparks exert a modulatory influence on the uridine 5′-triphosphate-induced translocation of the transcription factor NFAT3c (18). The role of Ca^{2+} sparks on the regulation of transcription factors in PASMCs has not been examined. However, since ET-1 is a potent mitogenic agonist involved in pulmonary vascular remodeling in pulmonary hypertension (7, 22) and is known to activate NFAT and other Ca^{2+}-sensitive transcription factors (28, 47) that mediate vascular cell proliferation, it is possible that Ca^{2+} sparks originating in the perinuclear regions may be involved in the regulation of gene expressions in PASMCs, perhaps in pulmonary hypertension.

Analysis of spatial distribution of Ca^{2+} sparks in PASMCs shows that the averaged Ca^{2+} spark frequency, number of sites, and number of spark per site are similar in the peripheral and the perinuclear sites, suggesting that these sites are equally capable of generating Ca^{2+} sparks. This is in contrast to the observation in rat portal vein myocytes that most of the Ca^{2+} sparks are generated from only one major FDS close to the nuclear envelope (19, 20). When Ca^{2+} spark activity is enhanced by caffeine or ET-1, the major increase is the number of active sites in both peripheral and perinuclear regions with only a moderate or no increase in number of spark per site, suggesting that agonist stimulation leads to the recruitment of more Ca^{2+} release units. Moreover, caffeine appears to exhibit some degree of differential regulation of peripheral Ca^{2+} sparks. The higher activity of Ca^{2+} spark in the peripheral region may suggest that the RyR subtypes in the peripheral SR Ca^{2+} stores are more sensitive to a subthreshold concentration of caffeine. Hot spots of more frequent discharge have been observed occasionally in a few highly responsive PASMCs, some of which acted as the initiation point for global Ca^{2+} waves or transients. The high activity of these sites could be related to local aggregation of RyRs, high regional SR density, and SR Ca^{2+} load.

Another interesting finding of the present study is the observation of prolonged perinuclear Ca^{2+} sparks. These Ca^{2+} sparks have a unique noninactivating kinetics, giving rise to a maintained plateau in the local Ca^{2+} transient lasting for an average of ~200 ms. This is in sharp contrast to the typical vascular and cardiac Ca^{2+} sparks, which terminate within 20–30 ms through the mechanisms of RyR inactivation and local Ca^{2+} depletion (4, 43). But they somewhat resemble the extremely prolonged nuclear Ca^{2+} release (PNCR) events identified most recently in intact and permeabilized rat myocytes (52). These PNCR in cardiac myocytes lasted on average for ~2 s and have greater diffusion of Ca^{2+} toward the center of the nucleus. Even though the prolonged perinuclear Ca^{2+} sparks in our PASMCs only account for <20% of all the perinuclear sparks recorded, the distinctive Ca^{2+} kinetics clearly suggests that some of the perinuclear RyRs possess gating mechanisms that differ from those of RyRs responsible for the typical fast inactivating peripheral and perinuclear Ca^{2+} sparks. It is tempting to speculate that these prolonged Ca^{2+} sparks originate from a specific RyR subtype or heterotetramer and are related to the regulation of nuclear functions. However, further future studies are required to explore these fascinating possibilities.

In conclusion, we have identified multiple RyR subtypes and characterized distinctive subpopulations of functional RyR-gated SR Ca^{2+} stores in adult rat intralobar PASMCs. The molecular complexity and spatial heterogeneity of RyRs may allow specific local Ca^{2+} regulation of diverse cellular functions in PASMCs.

ACKNOWLEDGMENTS

The authors thank Dr. Anita Umesh for helpful suggestions and discussions on the project. X.-R. Yang is supported by a postdoctoral fellowship from American Lung Association.

Present address of M.-J. Lin: Dept. of Physiology and Pathophysiology, Fujian Medical University, Fujian, People's Republic of China.

GRANTS

This work is supported in part by National Heart, Lung, and Blood Institute Grants HL-075134, HL-071835 and HL-063813 to J. S. K. Sham.

REFERENCES

1. **Archer SL, Huang JM, Reeve HL, Hampl V, Tolarova S, Michelakis E, and Weir EK.** Differential distribution of electrophysiologically distinct myocytes in conduit and resistance arteries determines their response to nitric oxide and hypoxia. *Circ Res* 78: 431–442, 1996.
2. **Bae YM, Park MK, Lee SH, Ho WK, and Earm YE.** Contribution of Ca^{2+}-activated K^+ channels and non-selective cation channels to membrane potential of pulmonary arterial smooth muscle cells of the rabbit. *J Physiol* 514: 747–758, 1999.
3. **Berridge MJ.** The AM and FM of calcium signalling. *Nature* 386: 759–760, 1997.
4. **Brochet DX, Yang D, Di Maio A, Lederer WJ, Franzini-Armstrong C, and Cheng H.** Ca^{2+} blinks: rapid nanoscopic store calcium signaling. *Proc Natl Acad Sci USA* 102: 3099–3104, 2005.
5. **Chun M, Liyanage UK, Lisanti MP, and Lodish HF.** Signal transduction of a G protein-coupled receptor in caveolae: colocalization of endothelin and its receptor with caveolin. *Proc Natl Acad Sci USA* 91: 11728–11732, 1994.
6. **Coussin F, Macrez N, Morel JL, and Mironneau J.** Requirement of ryanodine receptor subtypes 1 and 2 for Ca^{2+}-induced Ca^{2+} release in vascular myocytes. *J Biol Chem* 275: 9596–9603, 2000.
7. **DiCarlo VS, Chen SJ, Meng QC, Durand J, Yano M, Chen YF, and Oparil S.** ETA-receptor antagonist prevents and reverses chronic hypoxia-induced pulmonary hypertension in rat. *Am J Physiol Lung Cell Mol Physiol* 269: L690–L697, 1995.
8. **Dolmetsch R.** Excitation-transcription coupling: signaling by ion channels to the nucleus. *Sci STKE* 2003: PE4, 2003.
9. **Dolmetsch RE, Lewis RS, Goodnow CC, and Healy JI.** Differential activation of transcription factors induced by Ca^{2+} response amplitude and duration. *Nature* 386: 855–858, 1997.
10. **Dolmetsch RE, Pajvani U, Fife K, Spotts JM, and Greenberg ME.** Signaling to the nucleus by an L-type calcium channel-calmodulin complex through the MAP kinase pathway. *Science* 294: 333–339, 2001.
11. **Dolmetsch RE, Xu K, and Lewis RS.** Calcium oscillations increase the efficiency and specificity of gene expression. *Nature* 392: 933–936, 1998.
12. **Dreja K, Voldstedlund M, Vinten J, Tranum-Jensen J, Hellstrand P, and Sward K.** Cholesterol depletion disrupts caveolae and differentially impairs agonist-induced arterial contraction. *Arterioscler Thromb Vasc Biol* 22: 1267–1272, 2002.
13. **Fielding CJ.** Caveolae and signaling. *Curr Opin Lipidol* 12: 281–287, 2001.
14. **Fill M and Copello JA.** Ryanodine receptor calcium release channels. *Physiol Rev* 82: 893–922, 2002.
15. **Franzini-Armstrong C, Protasi F, and Ramesh V.** Comparative ultrastructure of Ca^{2+} release units in skeletal and cardiac muscle. *Ann NY Acad Sci* 853: 20–30, 1998.
16. **Franzini-Armstrong C, Protasi F, and Ramesh V.** Shape, size, and distribution of Ca^{2+} release units and couplons in skeletal and cardiac muscles. *Biophys J* 77: 1528–1539, 1999.
17. **Fujimoto T, Nakade S, Miyawaki A, Mikoshiba K, and Ogawa K.** Localization of inositol 1,4,5-trisphosphate receptor-like protein in plasmalemmal caveolae. *J Cell Biol* 119: 1507–1513, 1992.
18. **Gomez MF, Stevenson AS, Bonev AD, Hill-Eubanks DC, and Nelson MT.** Opposing actions of inositol 1,4,5-trisphosphate and ryanodine receptors on nuclear factor of activated T-cells regulation in smooth muscle. *J Biol Chem* 277: 37756–37764, 2002.
19. **Gordienko DV and Bolton TB.** Crosstalk between ryanodine receptors and IP(3) receptors as a factor shaping spontaneous Ca^{2+}-release events in rabbit portal vein myocytes. *J Physiol* 542: 743–762, 2002.
20. **Gordienko DV, Greenwood IA, and Bolton TB.** Direct visualization of sarcoplasmic reticulum regions discharging Ca^{2+} sparks in vascular myocytes. *Cell Calcium* 29: 13–28, 2001.
21. **Hakamata Y, Nakai J, Takeshima H, and Imoto K.** Primary structure and distribution of a novel ryanodine receptor/calcium release channel from rabbit brain. *FEBS Lett* 312: 229–235, 1992.
22. **Hassoun PM, Thappa V, Landman MJ, and Fanburg BL.** Endothelin 1: mitogenic activity on pulmonary artery smooth muscle cells and release from hypoxic endothelial cells. *Proc Soc Exp Biol Med* 199: 165–170, 1992.
23. **Jaggar JH.** Intravascular pressure regulates local and global Ca^{2+} signaling in cerebral artery smooth muscle cells. *Am J Physiol Cell Physiol* 281: C439–C448, 2001.
24. **Jaggar JH, Porter VA, Lederer WJ, and Nelson MT.** Calcium sparks in smooth muscle. *Am J Physiol Cell Physiol* 278: C235–C256, 2000.
25. **Jaggar JH, Wellman GC, Heppner TJ, Porter VA, Perez GJ, Gollasch M, Kleppisch T, Rubart M, Stevenson AS, Lederer WJ, Knot HJ, Bonev AD, and Nelson MT.** Ca^{2+} channels, ryanodine receptors and Ca^{2+}-activated K^+ channels: a functional unit for regulating arterial tone. *Acta Physiol Scand* 64: 577–587, 1998.
26. **Janiak R, Wilson SM, Montague S, and Hume JR.** Heterogeneity of calcium stores and elementary release events in canine pulmonary arterial smooth muscle cells. *Am J Physiol Cell Physiol* 280: C22–C33, 2001.
27. **Jiang D, Xiao B, Li X, and Chen SR.** Smooth muscle tissues express a major dominant negative splice variant of the type 3 Ca^{2+} release channel (ryanodine receptor). *J Biol Chem* 278: 4763–4769, 2003.
28. **Kawamura T, Ono K, Morimoto T, Akao M, Iwai-Kanai E, Wada H, Sowa N, Kita T, and Hasegawa K.** Endothelin-1-dependent coactivator of nuclear factors of activated T lymphocytes signaling associates with transcriptional coactivator p300 in the activation of the B cell leukemia-2 promoter in cardiac myocytes. *Circ Res* 94: 1492–1499 2004.
29. **Lee SH and Earm YE.** Caffeine induces periodic oscillations of Ca^{2+}-activated K^+ current in pulmonary arterial smooth muscle cells. *Pflügers Arch* 426: 189–198, 1994.
30. **Lesh RE, Nixon GF, Fleischer S, Airey JA, Somlyo AP, and Somlyo AV.** Localization of ryanodine receptors in smooth muscle. *Circ Res* 82: 175–185, 1998.
31. **Löhn M, Fürstenau M, Sagach V, Elger M, Schulze W, Luft FC, Haller H, and Gollasch M.** Ignition of calcium sparks in arterial and cardiac muscle through caveolae. *Circ Res* 81: 1034–1039, 2000.
32. **Lohn M, Jessner W, Furstenau M, Wellner M, Sorrentino V, Haller H, Luft FC, and Gollasch M.** Regulation of calcium sparks and spontaneous transient outward currents by RyR3 in arterial vascular smooth muscle cells. *Circ Res* 89: 1051–1057, 2001.
33. **Mironneau J, Coussin F, Jeyakumar LH, Fleischer S, Mironneau C, and Macrez N.** Contribution of ryanodine receptor subtype 3 to Ca^{2+} responses in Ca^{2+}-overloaded cultured rat portal vein myocytes. *J Biol Chem* 276: 11257–11264, 2001.
34. **Nelson MT, Cheng H, Rubart M, Santana LF, Bonev AD, Knot HJ, and Lederer WJ.** Relaxation of arterial smooth muscle by calcium sparks. *Science* 270: 633–637, 1995.
35. **Neylon CB, Richards SM, Larsen MA, Agrotis A, and Bobik A.** Multiple types of ryanodine receptor/Ca^{2+} release channels are expressed in vascular smooth muscle. *Biochem Biophys Res Commun* 215: 814–821, 1995.
36. **Otsu K, Willard HF, Khanna VK, Zorzato F, Green NM, and MacLennan DH.** Molecular cloning of cDNA encoding the Ca^{2+} release channel (ryanodine receptor) of rabbit cardiac muscle sarcoplasmic reticulum. *J Biol Chem* 265: 13472–13483, 1990.
37. **Pike LJ and Casey L.** Localization and turnover of phosphatidylinositol 4,5-bisphosphate in caveolin-enriched membrane domains. *J Biol Chem* 271: 26453–26456, 1996.
38. **Porter VA, Reeve HL, and Cornfield DN.** Fetal rabbit pulmonary artery smooth muscle cell response to ryanodine is developmentally regulated. *Am J Physiol Lung Cell Mol Physiol* 279: L751–L757, 2000.
39. **Porter VA, Rhodes MT, Reeve HL, and Cornfield DN.** Oxygen-induced fetal pulmonary vasodilation is mediated by intracellular calcium activation of K_{Ca} channels. *Am J Physiol Lung Cell Mol Physiol* 281: L1379–L1385, 2001.
40. **Remillard CV, Zhang WM, Shimoda LA, and Sham JSK.** Physiological properties and functions of Ca^{2+} sparks in rat intrapulmonary arterial smooth muscle cells. *Am J Physiol Lung Cell Mol Physiol* 283: L433–L444, 2002.
41. **Rhodes MT, Porter VA, Saqueton CB, Herron JM, Resnik ER, and Cornfield DN.** Pulmonary vascular response to normoxia and K_{Ca} channel activity is developmentally regulated. *Am J Physiol Lung Cell Mol Physiol* 280: L1250–L1257, 2001.
42. **Schlegel A, Volonte D, Engelman JA, Galbiati F, Mehta P, Zhang XL, Scherer PE, and Lisanti MP.** Crowded little caves: structure and function of caveolae. *Cell Signal* 10: 457–463, 1998.
43. **Sham JSK, Song LS, Chen Y, Deng LH, Stern MD, Lakatta EG, and Cheng H.** Termination of Ca^{2+} release by a local inactivation of ryanodine receptors in cardiac myocytes. *Proc Natl Acad Sci USA* 95: 15096–15101, 1998.

44. **Shannon TR, Guo T, and Bers DM.** Ca^{2+} scraps: local depletions of free [Ca^{2+}] in cardiac sarcoplasmic reticulum during contractions leave substantial Ca^{2+} reserve. *Circ Res* 93: 40–45, 2003.
45. **Shimoda LA, Sylvester JT, and Sham JSK.** Mobilization of intracellular Ca^{2+} by endothelin-1 in rat intrapulmonary arterial smooth muscle cells. *Am J Physiol Lung Cell Mol Physiol* 278: L157–L164, 2000.
46. **Smani T, Iwabuchi S, Lopez-Barneo J, and Urena J.** Differential segmental activation of Ca^{2+}-dependent CI-and K^+ channels in pulmonary arterial myocytes. *Cell Calcium* 29: 369–377, 2001.
47. **Sugimoto T, Haneda M, Sawano H, Isshiki K, Maeda S, Koya D, Inoki K, Yasuda H, Kashiwagi A, and Kikkawa R.** Endothelin-1 induces cyclooxygenase-2 expression via nuclear factor of activated T-cell transcription factor in glomerular mesangial cells. *J Am Soc Nephrol* 12: 1359–1368, 2001.
48. **Takeshima H, Nishimura S, Matsumoto T, Ishida H, Kangawa K, Minamino N, Matsuo H, Ueda M, Hanaoka M, Hirose T, and Numa S.** Primary structure and expression from complementary DNA of skeletal muscle ryanodine receptor. *Nature* 339: 439–445, 1989.
49. **Thorne GD and Paul RJ.** Effects of organ culture on arterial gene expression and hypoxic relaxation: role of the ryanodine receptor. *Am J Physiol Cell Physiol* 284: C999–C1005, 2003.
50. **Wang YX, Zheng YM, Abdullaev I, and Kotlikoff MI.** Metabolic inhibition with cyanide induces calcium release in pulmonary artery myocytes and *Xenopus* oocytes. *Am J Physiol Cell Physiol* 284: C378–C388, 2003.
51. **Xiao B, Masumiya H, Jiang D, Wang R, Sei Y, Zhang L, Murayama T, Ogawa Y, Lai FA, Wagenknecht T, and Chen SR.** Isoform-dependent formation of heteromeric Ca^{2+} release channels (ryanodine receptors). *J Biol Chem* 277: 41778–41785, 2002.
52. **Yang Z and Steele DS.** Characteristics of prolonged Ca^{2+} release events associated with the nuclei in adult cardiac myocytes. *Circ Res* 96: 82–90, 2005.
53. **Zhang WM, Yip KP, Lin MJ, Shimoda LA, Li WH, and Sham JSK.** Endothelin-1 activates Ca^{2+} sparks in PASMC: local Ca^{2+} signaling between inositol trisphosphate- and ryanodine-receptors. *Am J Physiol Lung Cell Mol Physiol* 285: L680–L690, 2003.